Applied Thermal Engineering 30 (2010) 2738–2745

Contents lists available at ScienceDirect

Applied Thermal Engineering

journal homepage: www.elsevier.com/locate/apthermeng

Numerical study on air-side performance of an integrated fin and micro-channel heat exchanger

Jiong Li [a], Shuangfeng Wang [a,*], Wang Cai [a], Weijun Zhang [b]

[a] Key Lab. of Enhance Heat Transfer and Energy Conversion, Ministry of Education, South China University of Technology, Guangzhou, Guangdong 510640, PR China
[b] Dongguan Gaobao Aluminium Mfy.Co. Ltd, 523275 PR China

ARTICLE INFO

Article history:
Received 21 February 2010
Accepted 26 July 2010
Available online 3 August 2010

Keywords:
Integrated fin and micro-channel heat exchanger
Heat transfer
Fin geometry
Numerical simulation

ABSTRACT

A new type of aluminum heat exchanger with integrated fin and micro-channel has been proposed. The air-side heat transfer and flow characteristics of the integrated fin and micro-channel heat exchanger are systematically analyzed by a 3D numerical simulation. The effect of flow depth, fin height, fin pitch and fin thickness at different Reynolds number is evaluated by calculating Colburn factor j and Fanning friction factor f. A parametric study method is used to analyze the fin designed parameters affecting the performance of the heat exchanger. The results show that the contribution ratio of the fin geometries in descending order is flow depth, fin pitch, fin height and fin thickness. The air-side performance of the integrated fin and micro-channel heat exchanger is compared with that of the multi-louver fin micro-channel heat exchanger and the wavy fin micro-channel heat exchanger.

1. Introduction

Micro-channel heat exchanger is a highly efficient air-cooled heat exchanger, and is one of the potential alternatives for replacing conventional finned tube heat exchangers [1], mainly used in industries such as automobiles, air conditioning and refrigeration at present. The louver fin flat tube heat exchanger and the wavy fin flat tube heat exchanger are the main forms of the micro-channel heat exchanger. For the fin and tube heat exchanger, the heat transfer is limited by the thermal resistance on the air-side. Thus, the louver fin and the wavy fin have been studied by a number of researchers.

Multi-louvered fin and flat tube heat exchangers have been performed experimentally by Kim and Bullard [2]. Forty five heat exchangers with different louver angles, fin pitches and flow depths were tested. The Colburn factor j and Fanning friction factor f correlations related to the heat transfer coefficient and pressure drop were generalized as functions of Reynolds number based on louver pitch according to the experimental data. Comparison results between the general correlations for j and f factors were analyzed. Chang et al. [3], and Chang and Wang [4,5] performed experimental studies on the air-side characteristics of louvered fin heat exchangers and developed correlations for j and f factors. Zhang and Tafti [6] focused on the effect of the Reynolds number, fin pitch, louver thickness, and louver angle on flow efficiency in multi-louvered fins. Their results showed that flow efficiency is strongly dependent on geometrical parameters, especially at low Reynolds numbers. The air-side thermal performance data were analyzed using the effectiveness-NTU method for the wavy fin flat tube heat exchanger by Dong et al. [7]. The effects of fin pitch, fin height and fin length on the performance of heat transfer and pressure drop were examined. The general correlations for j and f factors were derived, and they can predict 95% of the experimental data within ±10%. Computational fluid dynamics method has been also introduced into heat exchanger study. Malapure et al. [8] performed three-dimensional simulations to investigate different geometries with varying louver pitch, louver angle, fin pitch and tube pitch and for different Reynolds number. The air-side performance of heat exchanger is evaluated by calculating Stanton number and friction factor. They obtained designed curves to predict the heat transfer and the pressure drop for a given louver geometry. Hsieh [9] proposed successively increased or decreased louver angle patterns for multi-louver fin flat tube heat exchanger, and carried out a 3D numerical analysis on heat transfer and fluid flow to address this issue.

As mentioned above, micro-channel heat exchanger is a highly efficient air-cooled heat exchanger. However, the manufacture of traditional micro-channel heat exchanger is complex, and the cost is high. Its flat tube and the fin are welded together, so a long period of stress changes caused poor contact for the tube and the fin, and then affect the heat transfer performance. On the other hand, condensate removal and frost problems are the main factors

* Corresponding author. Tel.: +86 22236929.
E-mail address: sfwang@scut.edu.cn (S. Wang).

1359-4311/$ – see front matter © 2010 Elsevier Ltd. All rights reserved.
doi:10.1016/j.applthermaleng.2010.07.028

Nomenclature

C_p	specific heat at constant pressure, J kg^{-1} K^{-1}
C_T	correction number
D_h	hydraulic diameter, mm
f	Fanning friction factor
Fp	fin pitch, mm
Fd	flow depth, mm
Fh	fin height, mm
g_m	air flux flow at the minimum cross-section of the flow area, m s^{-1}
h	heat transfer coefficient, W m^{-2} K^{-1}
j	Colburn factor
JF	JF factor, dimensionless
k	thermal conductivity, W m^{-1} K^{-1}
Kc	abrupt contraction coefficient
Ke	abrupt expansion coefficient
L	the fin length along the air flow direction, m
Nu	average Nusselt number
Pr	Prandtl number
r_e	the number of effective replications
R	the difference between the maximum and the minimum SN ratio
Re_{D_h}	Reynolds number based on hydraulic diameter
S_β	mean variance for measured data
SN	signal-to-noise
S_T	sum of square for measured data
T	temperature, K
U	velocity, m s^{-1}
u, v, w	x, y, z velocity components, m s^{-1}
V_e	error sum of squares
x, y, z	Cartesian coordinates
ΔP	pressure drop, Pa

Greek symbols

δ	thickness, mm
μ	dynamic viscosity of air, Pa s
ρ	density, kg m^{-3}
θ	angle of fin
η	signal-to-noise ratio

Subscripts

in	inlet
w	wall
R	reference
upper	upper part of the computational domain

constraining its development and application. Therefore, a new type of aluminum heat exchanger with integrated fin and micro-channel has been proposed in this work. The photo of it is presented in Fig. 1. Compared with the traditional micro-channel heat exchanger, the new type of micro-channel heat exchanger has many advantages. Its processing is simple and the cost is low, and it doesn't occur that the fin will loose from the wall, and affect the heat transfer performance in use. There is no contact resistance as the fin and the flat tube are integrated. Its structure may be in favor of drainage and preventing frost as the fin has a certain angle, but it need to be studied further.

Since the heat transfer on the air-side is the major factor influencing heat exchanger performance, a three-dimensional CFD simulation is carried out to study the air-side heat transfer and flow characteristics of the integrated fin and micro-channel heat exchanger, to provide theoretical guidance for the fin geometry designing. The fin geometries are investigated in terms of Colburn j factor and Fanning friction f factor as a function of Re_{D_h}. The Taguchi method [10], known to be a very reasonable tool in a parametric study, is used to analyze the contribution ratio of fin geometry factor on the performance of the heat exchanger. Finally, the air-side heat transfer and flow characteristics of the integrated fin and micro-channel heat exchanger are compared with that of the traditional micro-channel heat exchanger published in literatures [2,7] .

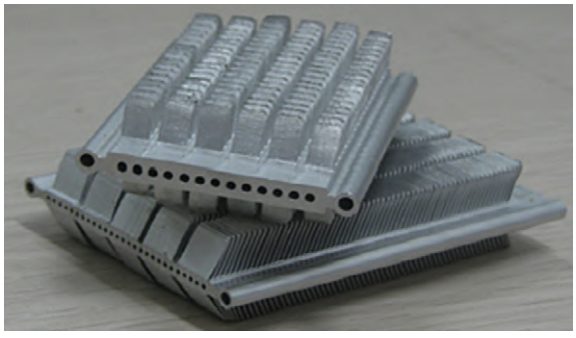

Fig. 1. Integrated fin and micro-channel heat exchanger core section.

2. Numerical simulation

2.1. Physical model

The map of the integrated fin and micro-channel heat exchanger core section is presented in Fig. 1. The schematic diagram of the integrated fin and micro-channel heat exchanger core section is shown in Fig. 2, which gives a top view and front view of the computation domain. Due to the symmetric and periodic arrangement, the section of the heat exchanger shown in Fig. 2 is selected as the computing units. The neighboring two fins' middle surfaces are selected as the upper and lower boundary of the computational element, respectively. The side surface of the fin and the tubes' middle surface are selected as the front and back boundary of the computational element, respectively. Because of the fin thickness, the air velocity profile is not uniform at the entrance of the channel formed by the fins' middle surfaces. The computational domain is extended upstream 0.25 times of the original heat transfer zone to ensure the velocity distribution uniform at the inlet of domain. The computational domain is also extended downstream 0.5 times of the original heat transfer zone so that fully developed boundary condition can be used at the outlet [11,12]. The elementary computational domain is presented in Fig. 3, in which x, y, z are stream wise, span wise and normal coordinates, respectively.

2.2. Grid generation

In this paper, the body-fitted coordinates are adopted, which helps to transform the complex computational computation domain in physical space into a simple domain in the computation space. The computational meshes are generated using Gambit, which is packaged with FLUENT software. The computational domain is divided into three parts in the flow direction: the upstream-extended region, the fin coil region and the upstream-extended region. The computational domain is discretized by

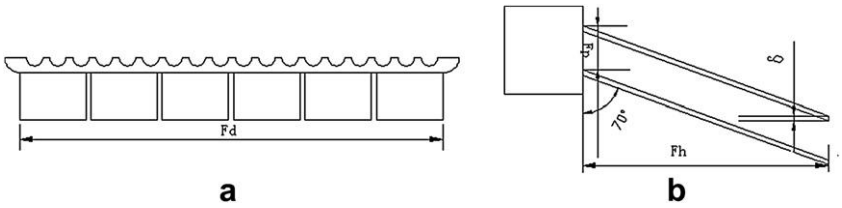

Fig. 2. Computational unit and definition of fin geometries: (a) top view; (b) front view.

non-uniform grids with the grids in the central-fin region being very fine while those in the extension domains being coarse to save the computing resource. The generated grid system is shown in Fig. 3.

2.3. Governing equations and boundary conditions

The CFD software FLUENT is used for the numerical simulation. The air flow between the neighboring fins is laminar owing to the low velocity and the small fin pitch. In the computation, the Reynolds number based on the inlet average velocity (1–7 m s^{-1}) and flow passage hydraulic diameter is below 2000. The flow is taken as steady, incompressible one [11,12]. The governing equations include continuity, momentum and energy equations for fluid region, conduction equation for solid region. The equations are expressed as follows [11,12]:

$$\text{Continuity equation}: \frac{\partial(\rho u_i)}{\partial x_i} = 0 \tag{1}$$

$$\text{Momentum equation}: \frac{\partial}{\partial x_i}(\rho u_i u_k) = \frac{\partial}{\partial x_i}\left(\mu\frac{\partial u_k}{\partial x_i}\right) - \frac{\partial p}{\partial x_k} \tag{2}$$

$$\text{Energy equation}: \frac{\partial}{\partial x_i}(\rho u_i T) = \frac{\partial}{\partial x_i}\left(\frac{k}{C_p}\frac{\partial T}{\partial x_i}\right) \tag{3}$$

Governing equations are discreted by means of the control volume method, and the convection term is discreted by adopting the power-law scheme. The coupling between pressure and velocity is conducted by the SIMPLE algorithm calculating the regional. Fin thickness and heat conduction in the fins are taken into account. The temperature distribution for the fins can be determined by solving the conjugate heat transfer problem in the computational domain. Similar treatments can be found in references [12,13]. The convergence criterion is that the normalized residuals are less than 10^{-6} for the flow equations and 10^{-8} for the energy equation.

The boundary conditions are described as follows:

At the inlet, velocity-inlet boundary condition: $u = u_{in}$, $T = T_{in}$, $v = \omega = 0$

At the upper and lower surface of the wind tunnel region (x–y planes), periodic boundary conditions:

$$\frac{\partial u}{\partial z} = \frac{\partial v}{\partial z} = 0,\ \omega = 0,\ \frac{\partial T}{\partial z} = 0\ (\text{extended region});\ u = v = \omega = 0,\ \frac{\partial T}{\partial z} = 0\ (\text{fin region})$$

At the front and back surface of the wind tunnel region (x–z planes), symmetry boundary condition:

$$\frac{\partial u}{\partial y} = \frac{\partial \omega}{\partial y} = 0,\ v = 0,\ \frac{\partial T}{\partial y} = 0$$

At the outlet boundary, outflow boundary condition:

$$\frac{\partial u}{\partial x} = \frac{\partial v}{\partial x} = \frac{\partial \omega}{\partial x} = \frac{\partial T}{\partial X} = 0$$

Fin surface region, interface: $u = v = \omega = 0$, $\partial T/\partial y = 0$

Tube region: $u = v = \omega = 0$, $T = T_w$

Geometric size and computational condition are listed in Table 1.

The numerical simulation model mentioned above is generally carried out for simulating air-side performance of the fin and tube

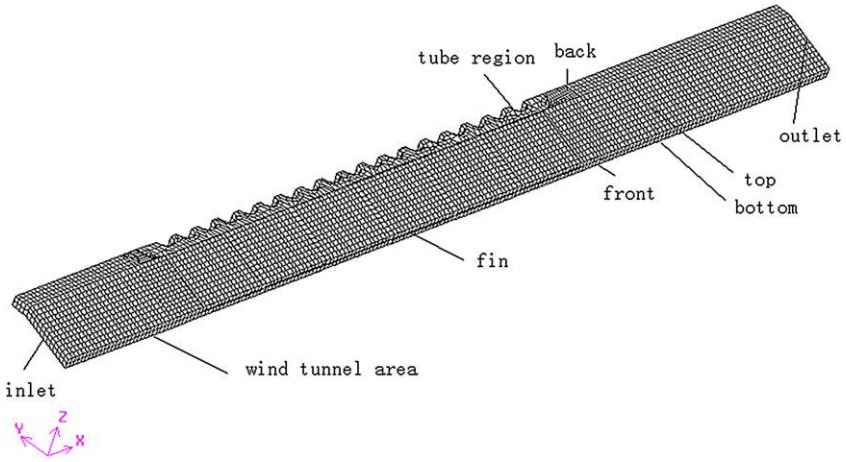

Fig. 3. Computational domain and grid system.

Table 1
Geometric sizes and computational conditions.

Parameter	Size or value
Flow depth	Fd
Fin height	Fh
Fin thickness	δ
Fin pitch	Fp
Tube diameter	0.8 mm
Tube spacing	0.78 mm
Flat tube thickness	3.5 mm
Fin angle θ	70°
Wall temperature T_w	333.15 K
Inlet temperature of air T_{in}	308 K
Inlet frontal velocity u_{in}	1–7 m s^{-1}

heat exchangers. It was presented by Tao et al. [13] and Leu et al. [14], agreements are very good for their results between simulation and experiment. Thus, this method is employed to simulate the integrated fin and micro-channel heat exchanger in the present work.

2.4. Parameter definition

To improve the model to be easily understood, Reynolds number, average Nusselt number, Colburn factor j, Fanning friction factor f are defined as follows:

$$Re = \frac{g_m D_h}{\mu} \tag{4}$$

$$Nu = \frac{hD_h}{k} \tag{5}$$

$$j = \frac{h}{g_m c_p} \cdot Pr^{\frac{2}{3}} \tag{6}$$

$$f = \frac{2\Delta P}{\rho U^2}\frac{D_h}{L} \tag{7}$$

To calculate the hydraulic diameter, the computational domain is divided into two equal parts along the z direction, and $D_h = 2D_{h,upper}$, $D_{h,upper} = 4(V_{upper}/S_{upper})$, V_{upper} is the upper part volume of the computational domain, S_{upper} is the upper part wetting area of the computational domain.

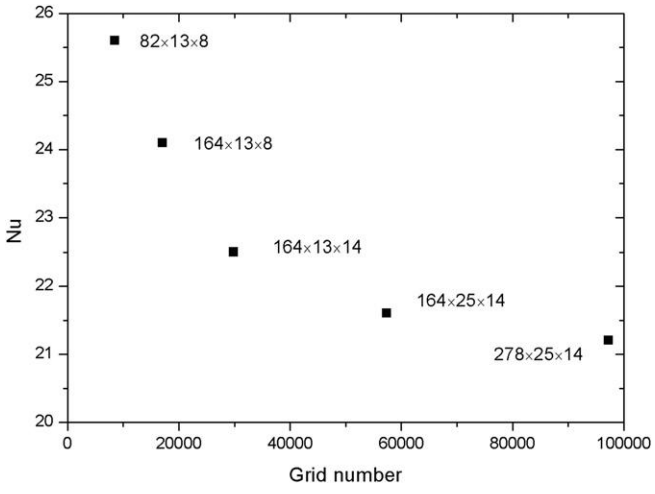

Fig. 4. Variation of the predicted Nusselt number with grid number.

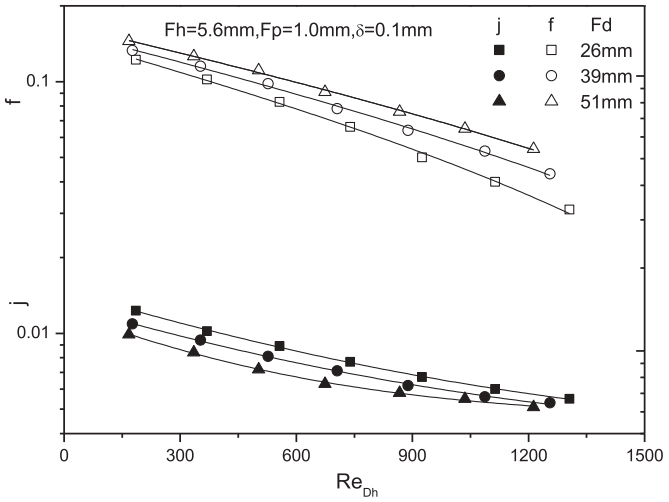

Fig. 5. Variation of j factor and f factor with flow depth.

2.5. Grid independence test

The grid independence test has been made, and the numerical results can be almost regarded as grid-independent as far as the average Nusselt number is convergenced. Taken the model of the heat exchanger with flow depth of 51 mm, fin height of 6.6 mm, fin pitch of 1.4 mm and fin thickness of 0.14 mm as an example, five grid systems were tested. They are 82 × 13 × 8, 164 × 13 × 8, 164 × 13 × 14, 164 × 25 × 14, 278 × 25 × 14. From Fig. 4, it can be seen that the solution of the grid system of 278 × 25 × 14 yields a Nusselt number about 1% lower than that of the grid system 164 × 25 × 14. So the grid system of 278 × 25 × 14 can be regarded as grid independent. Similar examinations are also conducted for the other cases.

3. Results and discussion

3.1. Heat transfer and flow characteristics

The air-side heat transfer and flow characteristics of the integrated fin and micro-channel heat exchanger with different fin geometries are presented in Figs. 5–12. The effect of the flow depth, the fin pitch, the fin height, and the fin thickness are analyzed, with Reynolds number below 2000. As is shown, the Colburn factor j and Fanning friction factor f all decrease with increasing Reynolds number within the range of examined Reynolds numbers.

Fig. 5 displays the effects of flow depth on the Colburn factor j and Fanning friction factor f of the fin for the integrated fin and micro-channel heat exchanger. It is noted that Fanning friction factor f increases with going up flow depth while j decreases with

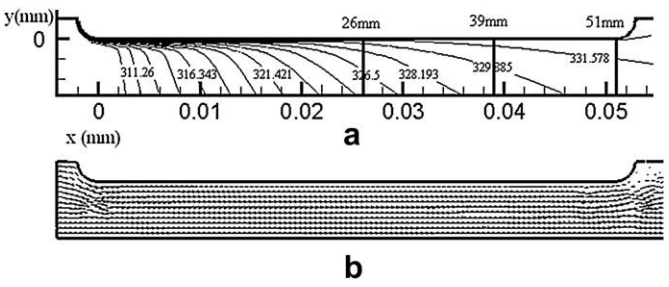

Fig. 6. Distribution of isothermal and streamline for Re = 882.9.

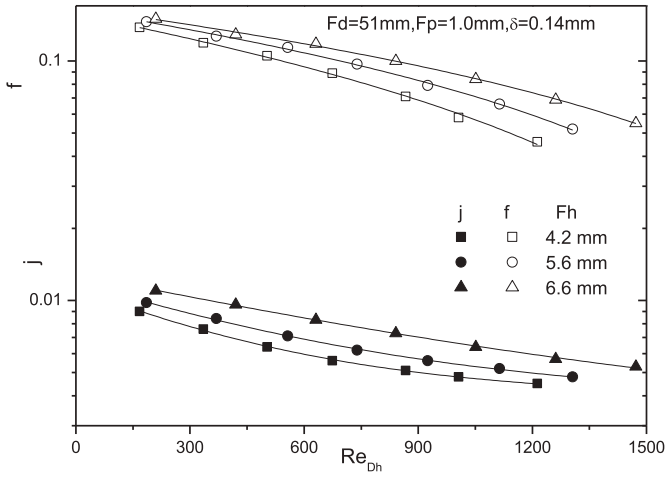

Fig. 7. Variations of *j* factor and *f* factor with fin height.

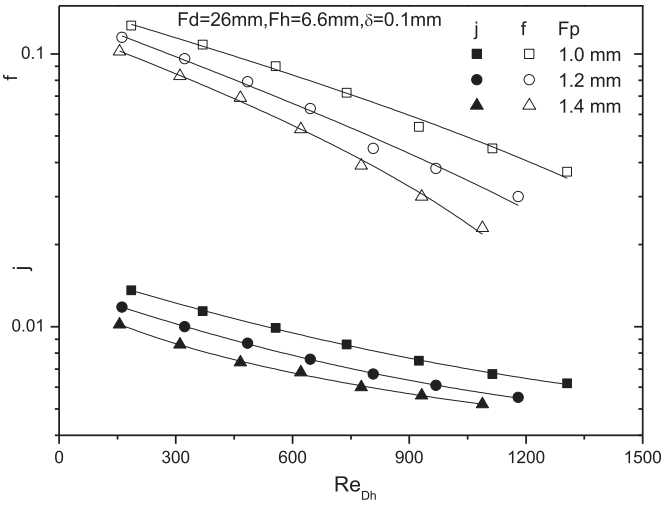

Fig. 9. Variation of *j* factor and *f* factor with fin pitch.

flow depth increasing. The trend of Colburn factor *j* and Fanning friction factor *f* as the function of flow depth is the same as that of Kim et al. [2] and Dong et al. [7]. As the flow depth increasing, the boundary layer develops more fully, and it's not in favor of heat transfer. Analyzed by the field synergy principle [15], Fig. 6 indicates that the isotherms are more or less normal to the local streamlines at the front part, implying good synergy between velocity and temperature field. Flowing to the back part of the domain, synergy between velocity and temperature field become worse and worse, the effect of heat transfer becomes worse.

Fig. 7 presents the *j* and *f* factors tend to increase with fin height increasing. The results are the same as that of the wavy fin and the louvered fin. From Fig. 8, it is shown that the intersection angle between local temperature field and the velocity flied decreases from 4.2 mm to 6.6 mm for the fin height, at the middle cross-section between the adjacent fins. It indicates synergy between velocity and temperature field becomes better as the fin height increasing. But the fin is not the higher, the better. The heat transfer effect and production cost must be considered together. There exists an optimal value of the fin height. For the fin height at the range of 4.2–6.6 mm, the fin height of 6.6 mm will be chosen.

The data points in Fig. 9 show the effect of fin pitch (1.0, 1.2, 1.4 mm) on the air-side thermal hydraulic performance of the heat exchangers with the same flow depth of 26 mm, fin height of 6.6 mm and fin thickness of 0.1 mm. At the same Reynolds number, the decrease of fin pitch results in the increase of *j* and *f* factors. As the fin pitch increases, the boundary layer interruption between the fins is delayed, and the heat transfer performance becomes worse. Fig. 10 shows the normal-averaged Nusselt number on the *z*–*x* plane, it can be seen Nusselt number for smaller fin pitch is higher than those for larger fin pitch as the boundary layer interruption between the fins is delayed. There are some peaks for normal-averaged Nusselt number in Fig. 10. Apparently, the interrupted fins break the boundary layer growth along the flow direction. While meeting a new interrupted fin, the boundary layer growth will appear a new leading edge for the flow, and the normal-averaged Nusselt number increases.

As increasing the fin thickness, the air flow will become more turbulent at the same fin pitch as the boundary layer interruption. Fig. 11 indicates the *j* and *f* factors increase with the fin thickness δ increasing. As can be seen from Fig. 12, the normal-averaged Nusselt number is higher for the fin thickness $\delta = 0.1$ mm than that of fin thickness $\delta = 0.115$ mm and $\delta = 0.14$ mm. The boundary layer interaction between the fins cannot be ignored for the plain fin while the fin pitch is small. The peaks for the normal-averaged Nusselt number are explained above.

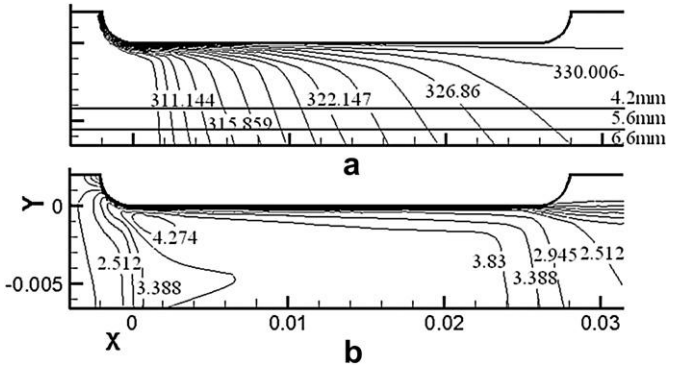

Fig. 8. Distribution of isothermal and velocity field for $Re = 518.4$.

3.2. Factor and level analyzed by Taguchi method [10,16]

The signal-to-noise ratio used in the analysis of Taguchi method, which is a measurement particularly used for process design. SN ratio can help engineers to find out which levels of control factors are more efficient. This study analyzes four factors (flow depth, fin height, fin pitch and fin thickness) affecting the air-side heat transfer and flow characteristics of the integrated fin and microchannel heat exchanger using Taguchi method. The factors and the levels are shown in Table 2.

$$\mathrm{JF} = \frac{j/j_R}{(f/f_R)^{1/3}} \tag{8}$$

JF is a dimensionless number which can effectively evaluate the thermal and dynamic performance of a heat exchanger since it includes both the *j* and the *f* factor.

SN ratio of the dynamic characteristics is defined as the following equations:

$$\mathrm{SN}(=\eta) = 10\lg\left(\frac{1}{r_e}\times\frac{(S_\beta - V_e)}{V_e}\right) \tag{9}$$

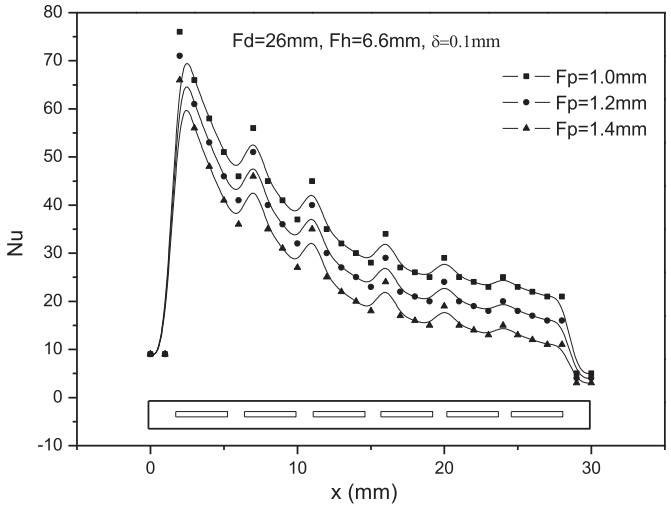

Fig. 10. Normal-averaged Nusselt number at z–x plane with different fin pitch.

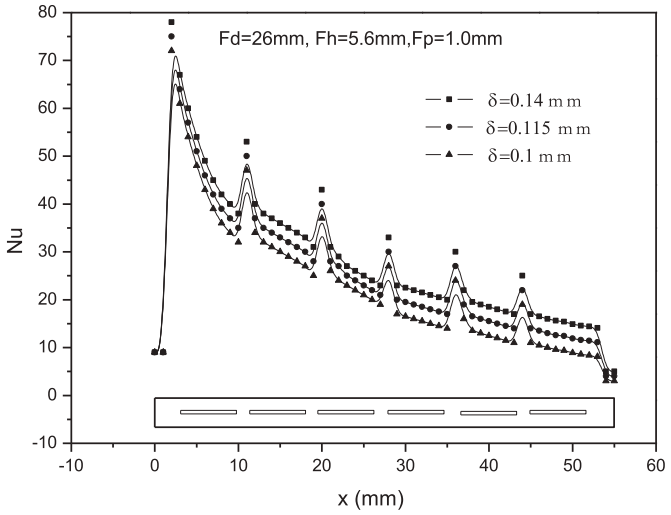

Fig. 12. Normal-averaged Nusselt number at z–x plane with different fin thickness.

Calculating the number of effective replications r_e and mean variance for measured data S_β:

$$r_e = \sum_{i=1}^{n}\left(Re_{D_h i} - \overline{Re_{D_h}}\right)^2 \tag{10}$$

$$S_\beta = \frac{1}{r_e}\left[\sum_{i=1}^{n}\left(Re_{D_h i} - \overline{Re_{D_h}}\right)\mathrm{JF}_i\right]^2 \tag{11}$$

Here, $Re_{D_h i}$ and JF_i represent the ith Reynolds number based integrated fin and the ith JF factor, respectively. There are seven test points of Re_{D_h} in this study.

Calculating the sum of square for measured data S_T, C_T is the correction number:

$$S_T = \sum_{l=1}^{n}\mathrm{JF}_i^2 - C_T \tag{12}$$

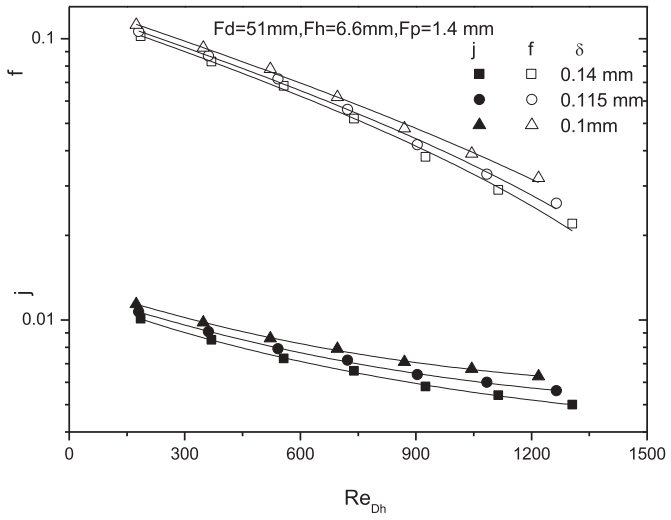

Fig. 11. Variation of j factor and f factor with fin thickness.

$$C_T = \frac{\left(\sum_{i=1}^{n}\mathrm{JF}_i\right)^2}{n} \tag{13}$$

Calculating the error sum of squares S_e and estimate of random error variance V_e:

$$S_e = S_T - S_\beta \tag{14}$$

$$V_e = \frac{S_e}{n-1} \tag{15}$$

$n-1$ represents the freedom.

The contribution ratio means the effect of each factor on the JF factor, namely the performance characteristics of a heat exchanger. This is calculated using R that indicates the difference between maximum and minimum of the SN ratio on each factor. As a result, the contribution ratio of each factor is obtained from the ratio of R corresponding to each factor to total R. Thus, the effect of each factor on the JF factor of the flow depth is enumerated as 39.06% for flow depth, 21.45% for fin height, 25.94% for fin pitch, and 13.58% for fin thickness as presented in Table 3. Fig. 13 shows the contribution ratio of the fin pitch is the largest and the fin thickness is the smallest among the considered factors. It is different from the analysis for the multi-louver fin flat tube heat exchanger by Qi et al. [16]. However, it is noted that the present results on the contribution ratio is limited to the effects of the four factors used in this study. Hence, to investigate the effects of factors other than those above, one can repeat a similar procedure.

Fig. 14 shows the SN ratio of four factors in every level, which can help us to choose the optimum fin geometry. The largest SN ratio level of all the levels on each factor has the best performance as mentioned above. For the flow depth, the level 1 (26 mm) is the

Table 2
levels of each factor.

Code	Factors (unit)	Level 1	Level 2	Level 3
A	Flow depth, Fd(mm)	26	39	51
B	Fin height, Fh(mm)	4.2	5.6	6.6
C	Fin pitch, Fp(mm)	1.0	1.2	1.4
D	Fin thickness δ (mm)	0.1	0.115	0.14

Table 3
Factional effect and contribution ratio for each factor.

Level		Control factor			
		A	*B*	*C*	*D*
SN ratio(η)	1	18.232	13.332	19.566	17.105
	2	15.612	14.186	18.084	16.472
	3	14.528	15.367	17.105	15.816
$R(\eta_{max} - \eta_{min})$	12.03	3.704	2.035	2.461	1.289
Contribution ratio (%)	100	39.03	21.45	25.49	13.58

best condition. As mentioned above, the performance of the front area has better heat transfer than the back area along the flow direction. For the most important parameter fin pitch, the smaller fin pitch has better heat transfer effect, so the fin pitch of 1.0 mm is optimal shown in Fig. 13. It also shows that the optimum size of fin height and fin thickness is 6.6 mm (C1) and 0.1 mm (D1), respectively. So the optimum condition is A1B3C1D1.

3.3. Comparison with traditional micro-channel heat exchanger

Fig. 15 displays the comparison of air-side heat transfer and flow characteristics for the integrated fin with that of the other type of fins. It is certain that the fins have the same geometry parameters: Fp = 1.0 mm, Fh = 6.6 mm, Fd = 26 mm, d = 0.1 mm. It is clear that the integrated fin has the interrupted plate fin while other fins are the multi-louvered fin and wavy fin. It can be seen from Fig. 15(a) that j and f of the integrated fin and are smaller than that of the multi-louvered fin and wavy fin at the same Reynolds number. Because the stronger disturbance is produced by the louvered fin and the wavy fin, heat transfer is enhanced and flow resistance also increases. Compared with that of the multi-louver [2] and the wavy fin [7], the maximum difference of Colburn j factor for the integrated fin is 24.3% and 20.1%, and the maximum difference of Fanning friction factor f the integrated fin is 28.6% and 20.5% at the same Reynolds number. Fig. 15(b) shows the comparison on the overall performance of the integrated fin with the multi-louvered fin and wavy fin by examining $j/[f^(1/3)]$ factor. When Reynolds number is below 1018.5, the performance of the integrated fin is worse than the multi-louvered fin and the wavy fin, because the boundary layer isn't broken strongly as the multi-louvered fin and wavy fin. With Reynolds number increasing up to 1018.5 and 1552.3, the performance of the integrated fin exceeds the wavy fin and the multi-louvered fin, respectively. As Reynolds number increases, the flow resistance play the dominant role for the $j/[f^(1/3)]$ factor gradually. The integrated fin has low flow resistance, so the overall performance becomes better and better. It is worth promoting and applying in

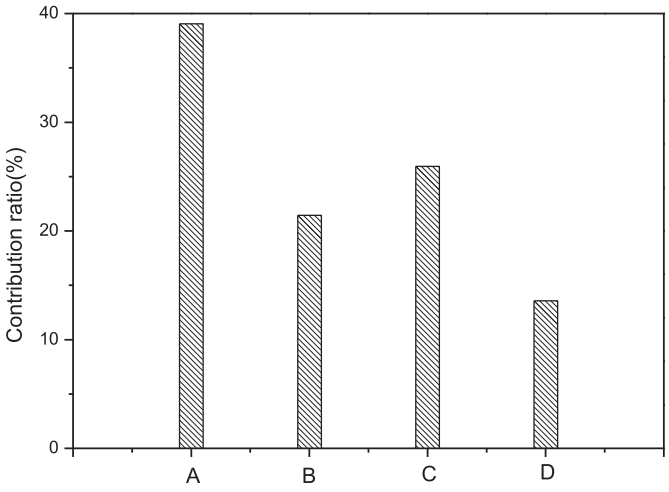

Fig. 13. Contribution ratio of every factor.

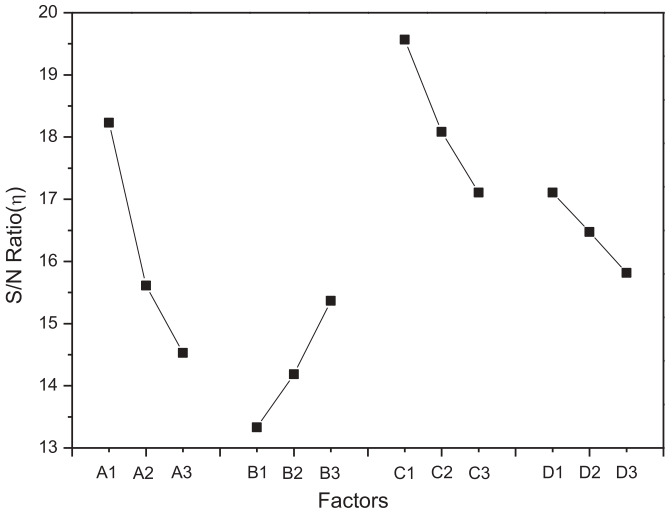

Fig. 14. SN ratio on every factor.

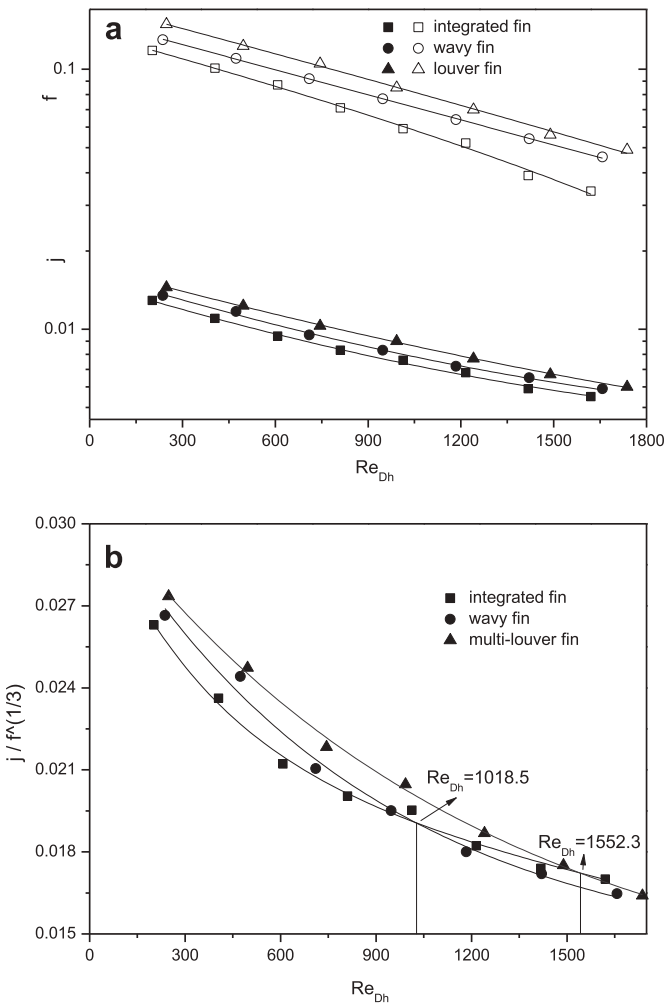

Fig. 15. Comparison of the heat transfer and flow characteristics with traditional micro-channel heat exchanger: (a) j and f; (b) $j/[f^(1/3)]$.

the automobiles, air conditioning, refrigeration, considering the performance and the advantages of the integrated fin and micro-channel heat exchanger.

4. Conclusions

In this study, an integrated fin and micro-channel heat exchanger has been proposed. The heat exchanger has the advantages of stable performance, easy drainage and preventing frost, low cost, light, compact, long service life. The air-side heat transfer and flow characteristics of the integrated fin and micro-channel heat exchanger are systematically analyzed by a 3D numerical simulation, the conclusions are as follows:

1. For Re number below 2000, both of the Colburn factor j and Fanning friction factor f increase with fin height and fin thickness increasing, and decrease with fin pitch increasing. As increasing the flow depth, j factor decreases but f factor increases.
2. According to analysis of the parameters with Taguchi method, descending order of the contribution ratio for the performance of the heat exchanger is flow depth, fin pitch, fin height and fin thickness. In the given size range, the heat exchanger with fin pitch of 1.0 mm, flow depth of 26 mm, fin height of 6.6 mm and fin thickness of 0.1 mm has the best performance.
3. At low Reynolds number, the air-side performance of integrated fin and micro-channel heat exchanger is worse than that of the multi-louver fin flat tube heat exchanger and the wavy fin flat tube heat exchanger. As Reynolds number increasing, the air-side performance of integrated fin and micro-channel heat exchanger is better than that of the multi-louver fin flat tube heat exchanger and the wavy fin flat tube heat exchanger.

Therefore, the integrated fin and micro-channel heat exchanger has good performance and so many advantages as described above, it is worth promoting the application and will have good prospects.

Acknowledgements

The authors acknowledge the financial support of funding from breakthroughs in key areas of Guangdong and Hong Kong Project (2007A090604002) and funding from NSFC, Granted No.50876033. The authors also wish to thank Dr. Zhang and Mr. Cai for providing valuable advice.

References

[1] R.L. Webb, Advances in air-cooled heat exchanger technology, in: Proceedings of the International Conference on Heat Exchangers for Sustainable Development, Lisbon, Portugal, 1998, pp. 677–692.
[2] M.H. Kim, W.C. Bullard, Air-side thermal hydraulic performance of multi-louvered fm aluminum heat exchangers, Int. J. Refrigeration 25 (2002) 390–400.
[3] Y. Chang, C. Wang, W. Chang, Heat transfer and flow characteristics of automotive brazed aluminum heat exchangers, ASHRAE Trans. 100 (1994) 643–652.
[4] Y. Chang, C. Wang, Air-side performance of brazed aluminum heat exchangers, J. Enhanced Heat Transf. 3 (1996) 15–28.
[5] Y. Chang, C. Wang, A generalized heat transfer correlation for louvered fin geometry, Int. J. Heat Mass Transf. 40 (1997) 533–544.
[6] X. Zhang, D.K. Tafti, Flow efficiency in multi-louvered fins, Int. J. Heat Mass Transf. 46 (2003) 1137–1150.
[7] J.Q. Dong, J.P. Chen, Z.J. Chen, Y.M. Zhou, W.F. Zhang, Heat transfer and pressure drop correlations for the wavy fin and flat tube heat exchangers, Appl. Therm. Eng. 27 (2007) 2066–2073.
[8] V.P. Malapure, K.M. Sushanta, A. Bhattacharya, Numerical investigation of fluid flow and heat transfer over louvered fins in compact heat exchanger, Int. J. Therm. Sci. 46 (2007) 199–211.
[9] C.T. Hsieh, J.Y. Jang, 3-D thermal-hydraulic analysis for louver fin heat exchangers with variable louver angle, Appl. Therm. Eng. 26 (2006) 1629–1639.
[10] T. Mori, The New Experimental Design: Taguchi's Approach to Quality Engineering. ASI Press, 1991.
[11] G.N. Xie, Q.W. Wang, Parametric study and multiple correlations on air-side heat transfer and friction characteristics of fin-and-tube heat exchangers with large number of large-diameter tube rows, Appl. Therm. Eng. 29 (2009) 1–16.
[12] J.M. Wu, W.Q. Tao, Investigation on laminar convection heat transfer in fin-and-tube heat exchanger in aligned arrangement with longitudinal vortex generator from the viewpoint of field synergy principle, Appl. Therm. Eng. 27 (2007) 2609–2617.
[13] Y.B. Tao, Y.L. He, J. Huang, Z.G. Wu, W.Q. Tao, Three-dimensional numerical study of wavy fin-and-tube heat exchangers and field synergy principle analysis, Int. J. Heat Mass Transf. 50 (2007) 1163–1175.
[14] J.S. Leu, Y.H. Wu, J.Y. Jang, Heat transfer and fluid flow analysis in plate-fin and tube heat exchangers with a pair of block shape vortex generators, Int. J. Heat Mass Transf. 47 (2004) 4327–4338.
[15] Z.Y. Guo, W.Q. Tao, R.K. Shah, The field synergy (coordination) principle and its applications in enhancing single phase convective heat transfer, Int. J. Heat Mass Transf. 48 (2005) 1797–1807.
[16] Z.G. Qi, J.P. Chen, Z.J. Chen, Parametric study on the performance of a heat exchanger with corrugated louvered fins, Appl. Therm. Eng. 27 (2007) 539–544.